Non-Abelian Geometric Dephasing

Kyrylo Snizhko,[1] Reinhold Egger,[2] and Yuval Gefen[1]
[1] *Department of Condensed Matter Physics, Weizmann Institute, Rehovot, Israel*
[2] *Institut für Theoretische Physik, Heinrich-Heine-Universität, D-40225 Düsseldorf, Germany*
(Dated: February 23, 2022)

We study the adiabatic dynamics of degenerate quantum states induced by loop paths in a control parameter space. The latter correspond to noisy trajectories if the system is weakly coupled to environmental modes. On top of conventional dynamic dephasing, we find a universal non-Abelian geometric dephasing (NAGD) contribution and express it in terms of the non-Abelian Berry connection and curvature. We show that NAGD implies either decay or amplification of coherences as compared to the coherences when only dynamic dephasing is present. The full NAGD matrix structure can be probed through interference experiments. We outline such a detection scheme for modified Majorana braiding setups.

arXiv:1904.11262v4 [cond-mat.mes-hall] 28 Jul 2020

Introduction.—Ever since the formulation of the Standard Model, non-Abelian gauge theories have played a central role in modern physics. In particular, concepts like the non-Abelian Berry connection and curvature [1] have been of key importance to such diverse topics as wave function dynamics in degenerate quantum systems [2], the fractional quantum Hall effect [3, 4], topological [5] and geometric [6, 7] quantum computation, nuclear quadrupole resonance [8], topological insulators [9, 10] and topologically ordered phases [11], degenerate Bloch bands in solids [12], synthetic non-Abelian gauge fields in ultracold atom systems [13, 14], or for a geometric understanding of Christoffel symbols in general relativity [15]. In particular, the non-Abelian theory generalizes the notion of adiabatic quantum transport from the non-degenerate Abelian case to N-fold degenerate state spaces with $N \geq 2$. In the Abelian case, a state picks up the celebrated geometric Berry phase when the time dependence of the Hamiltonian stems from adiabatically traversing a closed loop in parameter space [16]. For $N \geq 2$, the Berry phase factor is replaced by a unitary $N \times N$ Berry matrix $\mathcal{U}_B$, which again only depends on the geometry of the parameter loop [2].

It is of both fundamental and applied interest to understand what happens when the control parameters are subject to random fluctuations (noise) due to the system being weakly coupled to environmental modes. In the Abelian case, this problem has been extensively studied [17–25]. Most importantly, for a dissipative spin-1/2 system subject to a cyclic magnetic field trajectory, Refs. [23, 24] have predicted geometric dephasing contributions that depend on the sign of the winding (the trajectory orientation) along a closed path. This prediction has recently been confirmed [26] in superconducting nanocircuit experiments [27]. We here establish a theoretical framework for studying the non-Abelian adiabatic dynamics of *open* quantum systems. In particular, we show that universal geometric dephasing, described by a model-independent expression, is also present in the non-Abelian case. The nontrivial matrix structure associated with NAGD is responsible for richer physics and causes characteristic and experimentally observable differences compared to the Abelian counterpart. Experimental protocols for observing NAGD and confirming its distinctive features are given below, see also Ref. [28] for additional details. We illustrate our ideas for noisy Majorana braiding setups, where braiding is executed by running time-dependent protocols for the tunnel matrix elements between different pairs of Majorana bound states. Majorana braiding protocols are currently also of considerable experimental interest [29, 30]. From a general perspective, a thorough understanding of dephasing mechanisms in systems with degenerate subspaces has to include the NAGD contributions discussed here.

Physical origin of NAGD.—Before presenting explicit expressions for NAGD, we first qualitatively explain its essence. For a non-degenerate system, on top of the dynamic phase, $e^{i\varphi_d} = e^{-i\int dtE(t)}$, the adiabatic evolution of a state in the Hilbert space leads to a Berry phase factor $e^{i\varphi_B}$ [16]. For an open system, both the state trajectory and the energy fluctuate due to the influence of the environment. Upon averaging over such fluctuations, the phase $e^{i\varphi_d+i\varphi_B}$ will be replaced by $e^{i\varphi_d-\Gamma_{\rm dyn}T}e^{i\tilde{\varphi}_B-\Gamma_g}$ [23, 24]. With the time duration T of the protocol, the dynamic dephasing term, $\Gamma_{\rm dyn}T$, comes from fluctuations of the dynamic phase. Geometric dephasing is encoded by Γ_g, and there is a correction $\varphi_B \to \tilde{\varphi}_B$. Executing the same protocol in the opposite direction, we have $\tilde{\varphi}_B \to -\tilde{\varphi}_B$ but also $\Gamma_g \to -\Gamma_g$ [23, 24], resulting either in an amplification or a decrease of the state weight.

For a degenerate system, $e^{i\varphi_B}$ is replaced by a unitary matrix $\mathcal{U}_B$ which can always be diagonalized in an orthonormal basis. Under the adiabatic evolution, each basis state then simply gets multiplied by a phase factor. For an open system, the *averaged Berry matrix*, $\bar{\mathcal{U}}_B$, cannot be diagonalized in a single orthonormal basis anymore since the eigenbasis of $\mathcal{U}_B$ depends on the respective trajectory realization. However, diagonalization of $\bar{\mathcal{U}}_B$ is possible with *two* orthonormal bases, encoded by unitary matrices u and v. Under the adiabatic evolution, a vector in basis v is mapped to a corresponding vector in u, and multiplied by a real scaling factor $e^{-\Gamma_g}$ which de-

pends on the specific basis vector. We emphasize that such state mappings have to be understood with caution since one can in principle only average density matrices and not states [31]. However, many experimental observables for NAGD detection can be directly expressed in terms of the action of $\bar{\mathcal{U}}_B$ on an arbitrary initial state, see Ref. [28] and below. We now observe that for the time-reversed protocol, a vector in u is mapped to a vector in v and multiplied with the factor $e^{+\Gamma_g}$. We thus see that NAGD comes with a nontrivial matrix structure due to the existence of two bases. The details of the experimental protocol — and not only the orientation sense as in the Abelian case — will then determine whether NAGD implies an amplification or a suppression of coherences.

Non-Abelian Adiabatic Dynamics.—We consider a Hamiltonian $H(\boldsymbol{\lambda})$ that depends on d classical parameters, λ^μ, forming the vector $\boldsymbol{\lambda} = (\lambda^1, \ldots, \lambda^d)$. Suppose that for all relevant values of the parameters $\boldsymbol{\lambda}$, the Hamiltonian spectrum consists of M blocks with energy $E_j(\boldsymbol{\lambda})$ and degeneracy N_j. With a unitary, $U(\boldsymbol{\lambda})$, and a diagonal matrix, $D(\boldsymbol{\lambda}) = \sum_{j=1}^{M} E_j(\boldsymbol{\lambda}) P_j$, the Hamiltonian is given by $H(\boldsymbol{\lambda}) = U(\boldsymbol{\lambda}) D(\boldsymbol{\lambda}) U^\dagger(\boldsymbol{\lambda})$, where the P_j are diagonal matrices projecting to the respective block, $P_j P_k = \delta_{jk} P_j$. For now we focus on block $j = 1$ with degeneracy $N \equiv N_1$. By imposing a parameter protocol $\boldsymbol{\lambda}(t)$, we obtain a time-dependent Hamiltonian $H(t)$. We study closed loops, $\boldsymbol{\lambda}(0) = \boldsymbol{\lambda}(T)$, and without loss of generality assume $U(\boldsymbol{\lambda}(0)) = 1$. For $N = 1$, one has a non-degenerate system with an Abelian Berry phase, while for $N \geq 2$ one obtains the non-Abelian Berry matrix [2, 8].

Starting from an initial state in the N-fold degenerate subspace, $|\psi(0)\rangle = |\psi_0\rangle$, the Schrödinger equation, $i\partial_t |\psi(t)\rangle = H(t)|\psi(t)\rangle$, is solved by first transforming to the instantaneous eigenbasis, $|\psi(t)\rangle = U(\boldsymbol{\lambda}(t))|\tilde{\psi}(t)\rangle$. For sufficiently slow protocol $\boldsymbol{\lambda}(t)$, the adiabatic theorem implies that the state must remain in the degenerate subspace at all times. The final state follows as $|\tilde{\psi}(T)\rangle = \mathcal{U}|\tilde{\psi}(0)\rangle$, with $\mathcal{U} = e^{-i\int_0^T dt E_1} \mathcal{U}_B$ and the $N \times N$ Berry matrix [2, 8]

$$\mathcal{U}_B = \mathcal{T} e^{-\int_0^T dt\ \dot{\lambda}^\mu(t) A_\mu(\boldsymbol{\lambda}(t))} = \mathcal{P} e^{-\oint d\lambda^\mu A_\mu}. \tag{1}$$

Summation over repeated indices is always implied, $\mathcal{T}$ ($\mathcal{P}$) denotes time (path) ordering, and with the shorthand $\partial_\mu = \partial_{\lambda^\mu}$, the non-Abelian Berry connection is given by [1]

$$A_\mu(\boldsymbol{\lambda}) = P_1 U^\dagger(\boldsymbol{\lambda}) \partial_\mu U(\boldsymbol{\lambda}) P_1 = -A_\mu^\dagger(\boldsymbol{\lambda}). \tag{2}$$

As a path-ordered Wilson loop amplitude, $\mathcal{U}_B$ evidently is of purely geometric origin.

Coupling to environment.—We now allow for weak fluctuations of the control parameters, $\boldsymbol{\lambda}(t) \to \boldsymbol{\lambda}(t) + \delta\boldsymbol{\lambda}(t)$, around a base trajectory $\boldsymbol{\lambda}(t)$ [32]. Here the noise trajectory $\delta\boldsymbol{\lambda}(t)$ can be generated from classical fluctuations of the control parameters and/or from a coupling of the system to a quantum bath. In the latter case, $\delta\boldsymbol{\lambda}(t)$ represents operators acting on the bath Hilbert space which entangle the system with the bath and result in a non-unitary time evolution of the system. To simplify the analysis, we treat typical system-bath couplings in Markov-Born approximation [31], where one obtains Gaussian statistics with vanishing mean, $\langle \delta\lambda^\mu(t) \rangle = 0$, and the correlation function

$$\langle \delta\lambda^\mu(t) \delta\lambda^\nu(t') \rangle = \sigma^{\mu\nu} \delta_{\tau_c}(t - t'). \tag{3}$$

The real positive $d \times d$ matrix with components $\sigma^{\mu\nu} = \sigma^{\nu\mu}$ contains the noise amplitudes and $\delta_{\tau_c}(t - t')$ is a δ-function broadened on the scale of the noise correlation time τ_c [33]. We note in passing that artificially generated classical noise with such properties has been employed experimentally for the Abelian case [26], allowing for in-detail investigations of noise-related effects. In what follows, we denote the typical size of $\sigma^{\mu\nu}$, e.g., the largest eigenvalue, by σ. For simplicity, we assume that λ^μ (and thus also $\sigma^{\mu\nu}$ and σ) carries energy units. Below we impose three conditions: (i) The noise correlation time τ_c is short against the protocol duration T. (ii) The evolution does not mix block 1 with other blocks. With the minimal energy difference $\mathcal{E}$ between E_1 and other eigenenergies, this implies $\mathcal{E}\tau_c \gg 1$. (iii) The system-bath coupling is weak, $\sigma \ll \mathcal{E}$. In summary, we arrive at the inequality chain

$$\mathcal{E}T \gg \mathcal{E}\tau_c \gg 1 \gg \sigma/\mathcal{E}. \tag{4}$$

Averaged Berry matrix.—Consider first a single realization of the control parameter trajectory, $\boldsymbol{\lambda}(t) + \delta\boldsymbol{\lambda}(t)$. Expanding Eq. (1) in powers of $\delta\lambda^\mu$ and using Eq. (4), we obtain $\mathcal{U} = e^{-i\int_0^T dt E_1(\boldsymbol{\lambda}(t) + \delta\boldsymbol{\lambda}(t))} \mathcal{U}_B$, with the Berry matrix

$$\mathcal{U}_B = \mathcal{P} \exp \oint d\lambda^\mu \left[-A_\mu + \delta\lambda^\nu F_{\mu\nu} + \mathcal{O}(\delta\lambda^2) \right], \tag{5}$$

and the non-Abelian Berry curvature (or field strength) tensor [1],

$$F_{\mu\nu}(\boldsymbol{\lambda}) = \partial_\mu A_\nu - \partial_\nu A_\mu + [A_\mu, A_\nu] = -F_{\mu\nu}^\dagger. \tag{6}$$

We next perform the Gaussian average over the fluctuations $\delta\lambda^\mu(t)$ according to Eq. (3). We then obtain

$$\bar{\mathcal{U}} = e^{-i\int_0^T dt E_1} e^{-\frac{1}{2}\int_0^T dt\ \sigma^{\mu\nu} \partial_\mu E_1 \partial_\nu E_1} \bar{\mathcal{U}}_B, \tag{7}$$

where the averaged Berry matrix can again be expressed as a path-ordered exponential,

$$\bar{\mathcal{U}}_B = \mathcal{P} \exp \oint d\lambda^\mu \left(-A_\mu + i\sigma^{\nu\rho} F_{\nu\mu} \partial_\rho E_1 \right), \tag{8}$$

and thus also represents a geometric contribution. The terms dropped in the exponent of Eq. (8) are of order $\mathcal{O}\left(\frac{1}{\mathcal{E}T}, \frac{\sigma^2}{\mathcal{E}^2}, \frac{\sigma}{\mathcal{E}^2 \tau_c} \right)$ [28] and thus vanish according to

Eq. (4). The first term in Eq. (7) contains the dynamic phase. The second term describes dynamic dephasing, with a trivial matrix structure in the N-dimensional Hilbert space of block 1 and the exponent $\Gamma_{\rm dyn}T \sim \sigma T$. Note that this term stays invariant under the time reversal of the protocol, $\boldsymbol{\lambda}'(t) = \boldsymbol{\lambda}(T-t)$. The nontrivial matrix structure of $\bar{\mathcal{U}}$ is encoded by the averaged Berry matrix $\bar{\mathcal{U}}_B$ in Eq. (8), which contains both the non-Abelian Berry phase of the base path and an extra piece from the interplay of dynamic ($\sim \partial_\rho E_1$) and geometric ($\sim F_{\nu\mu}$) phase fluctuations. Noting that $(iF_{\nu\mu})^\dagger = iF_{\nu\mu}$, this term yields a Hermitian contribution from Eq. (8) which is responsible for geometric dephasing. We stress that for classical fluctuations $\delta\boldsymbol{\lambda}$, a non-unitary matrix $\mathcal{U}_{\mathcal{B}}$ emerges only after performing an average over fluctuation realizations. Finally, since replacing $\boldsymbol{\lambda}(t) \to \boldsymbol{\lambda}'(t)$ reverses the path ordering and flips the sign of $d\lambda^\mu$, the time-reversed protocol has the averaged Berry matrix $\bar{\mathcal{U}}_B^{-1}$.

Polar decomposition.—The non-unitary $N \times N$ matrix $\bar{\mathcal{U}}_B$ admits the singular value decomposition $\bar{\mathcal{U}}_B = u\Lambda v^\dagger$ [34], where the unitaries u and v encode the two bases introduced above. The diagonal matrix Λ describes NAGD and contains the respective real scaling factors $e^{-\Gamma_g}$. We thus have the polar decomposition [34]

$$\bar{\mathcal{U}}_B = VR, \quad V = uv^\dagger, \quad R = v\Lambda v^\dagger = R^\dagger, \tag{9}$$

where V is a unitary rotation and R is a positive semi-definite Hermitian matrix. For generic non-Abelian systems, one has $[V, R] \neq 0$. We will see below that the non-commutativity of V and R has profound and experimentally observable consequences. One can diagonalize the unitary rotation, $V = w\Phi w^\dagger$, with a unitary w and a diagonal matrix Φ containing phase factors. Hence $\bar{\mathcal{U}}_B$ is composed of (i) a real scaling transformation (Λ) applied in the basis encoded by v, followed by (ii) a phase multiplication (Φ) in the basis encoded by w. We next observe that the averaged Berry matrix for the reversed protocol, $\bar{\mathcal{U}}_B^{-1}$, has the polar decomposition

$$\bar{\mathcal{U}}_B^{-1} = \tilde{V}\tilde{R}, \quad \tilde{V} = V^\dagger, \quad \tilde{R} = u\Lambda^{-1}u^\dagger = \tilde{R}^\dagger. \tag{10}$$

While the unitary rotation is simply $\tilde{V} = V^\dagger$, the Hermitian matrix $\tilde{R}$ contains the diagonal matrix Λ^{-1} (characteristic of geometric dephasing) but in a different basis than for the forward direction, cf. Eq. (9). The matrix structure of NAGD thus plays a crucial role when comparing results for different directions of the protocol.

NAGD detection by Mach-Zehnder interferometry.—The conceptually simplest setup to probe $\bar{\mathcal{U}}_B$ is the Mach-Zehnder interferometer sketched in Fig. 1. Consider a particle with an internal spin-S degree of freedom (where $S \geq 1$), which is prepared in the initial state $|\psi(0)\rangle = |\psi_0\rangle$. In one arm of the interferometer, the spin dynamics evolves according to the Hamiltonian $H(\boldsymbol{\lambda}(t) + \delta\boldsymbol{\lambda}(t))$, while in the other arm, $H = 0$. The time of flight is then given by T. Averaging over the parameter fluctuations $\delta\boldsymbol{\lambda}$, i.e., over many experimental runs, the probability for the particle to appear at the respective detector $D_{1,2}$ in Fig. 1 is given by $\bar{P}_{1,2} = (1 \pm \mathrm{Re}\langle\psi_0|\bar{\mathcal{U}}|\psi_0\rangle)/2$, with $\bar{\mathcal{U}}$ in Eqs. (7) and (8). It stands to reason that by repeating such an experiment for many different initial states $|\psi_0\rangle$, the full matrix structure of $\bar{\mathcal{U}}$, and thus of $\bar{\mathcal{U}}_B$, can be determined. Natural candidates for such experiments are given by $S = 3/2$ nuclei experiencing nuclear quadrupole resonance [35, 36], where Berry connection and curvature expressions can be found in Ref. [8].

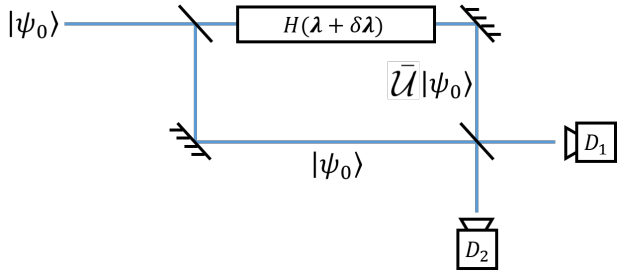


FIG. 1. An interferometric setup for observing NAGD. For details, see main text.

Two-block interference for NAGD detection.—In experiments on condensed-matter systems featuring Abelian [26, 27] or non-Abelian Berry phases [9, 10, 37, 38], it is usually not possible to probe spatial superpositions as shown in Fig. 1. Fortunately, in such cases, one may employ a different interference experiment as described next. Our interference scheme takes into account two blocks ($j = 1, 2$), with the respective energy $E_j(\boldsymbol{\lambda})$, degeneracy N_j, and projector P_j. Let us start from an arbitrary initial state within the two blocks, $(P_1+P_2)|\psi(0)\rangle = |\psi(0)\rangle$, and run a parameter loop protocol with Hamiltonian $H(\boldsymbol{\lambda}(t)+\delta\boldsymbol{\lambda}(t))$ as before. At time $t = T$, the expectation value of an operator of the form $\boldsymbol{M} = P_1\boldsymbol{M}^{(12)}P_2 + \mathrm{H.c.}$ is measured. (Block-diagonal contributions, e.g., $P_1\boldsymbol{M}^{(11)}P_1$, do not cause NAGD signatures [28].) For a given parameter trajectory, we thus obtain $\mathcal{M} = \langle\psi(T)|\boldsymbol{M}|\psi(T)\rangle$. Averaging this measurement over fluctuations, the result can be cast as the expectation value of an operator $\bar{\boldsymbol{M}}$ in the *known* initial state,

$$\bar{\mathcal{M}} = \langle\psi(0)|\bar{\boldsymbol{M}}|\psi(0)\rangle, \quad \bar{\boldsymbol{M}} = \big(\bar{\mathcal{U}}^{(1)}\big)^\dagger \boldsymbol{M}^{(12)}\bar{\mathcal{U}}^{(2)} + \mathrm{H.c.}, \tag{11}$$

with $\bar{\mathcal{U}}^{(j)} = e^{-i\int_0^T dt\left[E_j - \frac{i}{2}\sigma^{\mu\nu}\partial_\mu E_j \partial_\nu \tilde{E}_j\right]}\bar{\mathcal{U}}_B^{(j)}$. The averaged Berry matrices $\bar{\mathcal{U}}_B^{(j)}$ are defined as in Eq. (8) but with the Berry connection $A_\mu^{(j)}$ and curvature $F_{\nu\mu}^{(j)}$ of the respective block, see Eqs. (2) and (6), and using $E_1 \to \tilde{E}_j$ with $\tilde{E}_1 = -\tilde{E}_2 = E_1 - E_2$. Importantly, the operator $\bar{\boldsymbol{M}}$ in Eq. (11) contains the averaged Berry matrices. The above protocol thus offers experimental access to the physics associated with NAGD. In particular, by system-

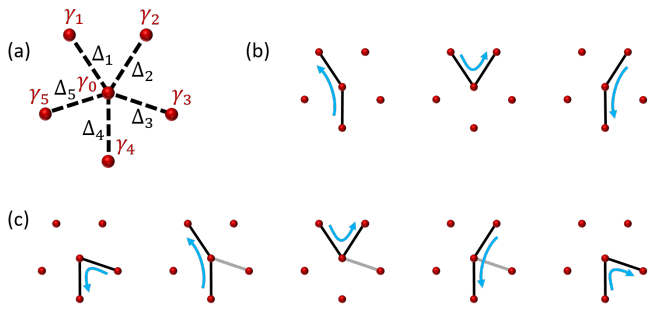


FIG. 2. Schematic setup for NAGD detection using noisy Majorana braiding protocols. (a) Five-star Majorana setup with tunnel couplings $\Delta_{j=1,\ldots,5}$ between Majorana operators γ_0 and γ_j. (b) Three-star setup with $\Delta_3 = \Delta_5 = 0$ (solid black lines indicate $\Delta_j > 0$) and topologically protected Majorana braiding protocol [29, 39, 40]. The shown sequence implies an exchange of γ_1 and γ_2. For instance, in the first step, one starts with only $\Delta_4 > 0$. The blue arrow then means that $\Delta_4(t)$ is slowly reduced to zero while $\Delta_1(t)$ is simultaneously ramped up. (c) Elementary steps for the NAGD detection protocol, where $\Delta_5 = 0$ at all times. The grey solid line indicates an additional coupling $\Delta_3' \neq 0$ needed for generating NAGD. For a full description of the protocol, see main text.

atic variation of the initial state $|\psi(0)\rangle$ and of the measured operator $\boldsymbol{M}$, one can map out the averaged Berry matrices. We emphasize that such a detection scheme relies on interference between two different blocks. Let us also remark that for $N_1 = N_2$, a powerful spin-echo type variant of this protocol exists where dynamic phases drop out completely [28]. Below we discuss a concrete example for such a protocol using modified Majorana braiding setups.

Noisy Majorana braiding setup.—Let us next consider the five-star Majorana setup in Fig. 2(a) which we model by the Hamiltonian $H_M(t) = i\gamma_0 \sum_{j=1}^{5} \Delta_j(t)\gamma_j$, where the real-valued tunnel couplings Δ_j correspond to $\boldsymbol{\lambda}(t)$. They can be tuned, e.g., by electric gates. The Majorana operators $\gamma_k = \gamma_k^\dagger$ satisfy the anticommutator algebra $\{\gamma_k, \gamma_l\} = 2\delta_{kl}$ [29]. Since total fermion number parity is conserved, we choose, say, the even parity sector, corresponding to a four-dimensional Hilbert space. H_M has the two-fold degenerate energy levels $E_\pm = \pm\mathcal{E}/2$ with $\mathcal{E} = 2\sqrt{\sum_j \Delta_j^2}$, corresponding to E_1 and E_2 above. We assume that the fluctuations $\delta\Delta_j(t)$ are uncorrelated for different tunnel links. Since tunnel couplings Δ_j are exponentially sensitive to fluctuations, the latter act in a multiplicative way, i.e., $\delta\Delta_j(t) \sim \Delta_j(t)$ [41, 42], and Eq. (3) gives

$$\langle \delta\Delta_j(t)\delta\Delta_k(t')\rangle = \kappa_j \Delta_j^2(t)\delta_{jk}\delta_{\tau_c}(t-t'), \qquad (12)$$

where Eq. (4) implies $\kappa_j\mathcal{E} \ll 1$ for the noise amplitudes κ_j. We assume below that only $\kappa_4 \neq 0$, but see Ref. [28] for the general case.

Let us now recall that Majorana braiding is conventionally discussed for a three-star setup [29, 39–44]. The corresponding braiding protocol is shown in Fig. 2(b), where at all times only two $\Delta_j(t)$ are non-zero. As a consequence, even when including the noise in Eq. (12), the *geometric* trajectory in the relevant parameter space $\{\Delta_j(t)/\mathcal{E}\}$ does not fluctuate. According to Eq. (8), NAGD is due to cross-correlations of energy fluctuations and geometric trajectory fluctuations. The absence of the latter thus implies the absence of NAGD, reflecting the topological protection of this braiding scheme [28]. By contrast, for the same protocol, the presence of an extra coupling ($\Delta_3' \neq 0$) removes the protection and allows for geometric trajectory fluctuations. We thereby obtain an appealing candidate for NAGD detection. The sequence in Fig. 2(c) provides an example, where during intermediate steps, we set $\Delta_3(t) = \Delta_3' \neq 0$. Even though Δ_3' does not fluctuate, geometric trajectory fluctuations can then develop from $\delta\Delta_4(t)$ contributions.

Spin-echo protocol for the Majorana setup.—We now discuss the NAGD detection protocol depicted in Fig. 2(c). We start from the initial state $|\psi_0\rangle \sim |0_{12}0_{03}0_{45}\rangle + |1_{12}1_{03}0_{45}\rangle$, where $|n_{jk}\rangle$ with $n_{jk} = (p_{jk}+1)/2 = 0, 1$ encodes the eigenvalue $p_{jk} = \pm 1$ of the Majorana parity operator $\hat{p}_{jk} = i\gamma_j\gamma_k$. We note that $|\psi_0\rangle$ can be prepared from $|0_{12}0_{03}0_{45}\rangle$ by measuring the parity operator $\hat{p}_{02}$ with outcome $p_{02} = -1$ [45]. Readout of Majorana parities can be performed as described in Refs. [28, 45–50]. One then runs (i) the sequence shown in Fig. 2(c), followed by (ii) the time-reversed sequence but with $\Delta_3' = 0$. At this point ($t = T$), (iii) one applies the flip operator $\hat{p}_{02} = i\gamma_0\gamma_2$ which will effectively exchange both blocks. Also for this operation, implementation proposals are available [45, 47–50]. We then, (iv) and (v), simply repeat steps (i) and (ii). The protocol ends by (vi) applying the flip operator $\hat{p}_{02}$ again. The Majorana parities $\hat{p}_{0j} = i\gamma_0\gamma_j$ are then measured in the final state, and the results are subsequently averaged over the noise to yield the expectation values $\bar{p}_{0j}$. Fortunately, this problem is simple enough to admit analytical predictions [28]. We can thus avoid a full-fledged numerical analysis of path-ordered expressions for the averaged Berry matrices which is required in most other applications. For overall orientation sense $\eta = \pm$ of the protocol, using $\cos\alpha = 2\Delta_3'/\mathcal{E}$ and $\beta = (\pi/4)\cos\alpha$, we find

$$\begin{aligned} \bar{p}_{01} &= e^{-4\Gamma_{\rm dyn}T}\mathcal{O}(\zeta^2), \quad \bar{p}_{03} = \bar{p}_{05} = 0, \\ \bar{p}_{02} &= e^{-4\Gamma_{\rm dyn}T}\left[-1 + 2\eta\zeta\sin(4\beta) + \mathcal{O}(\zeta^2)\right], \\ \bar{p}_{04} &= -8e^{-4\Gamma_{\rm dyn}T}\zeta\sin^2\beta + \mathcal{O}(\zeta^2), \end{aligned} \qquad (13)$$

with a dynamic dephasing rate $\Gamma_{\rm dyn} \sim \kappa_4\mathcal{E}^2$ and the dimensionless NAGD parameter $\zeta = \frac{3\pi}{16}\kappa_4\mathcal{E}\sin^4\alpha\cos\alpha$. While the contribution $\sim \zeta$ to $\bar{p}_{02}$ depends on $\eta = \pm$ in the same manner as expected for Abelian geometric dephasing, the average $\bar{p}_{04}$ vanishes without noise and otherwise does *not* change sign under $\eta \to -\eta$. This last feature, in particular, represents compelling evidence for

NAGD [28].

Conclusions.—We have shown that the adiabatic quantum dynamics within a degenerate subspace of an open system will contain universal NAGD contributions. The unique matrix structure of NAGD allows for its clear-cut identification using interference experiments. Interesting directions for future work include extensions to other topological entities (e.g., parafermions or non-Abelian quasi-particles in quantum Hall setups), applications to weak anti-localization in condensed-matter systems with a non-Abelian Berry connection, as well as the study of non-adiabatic corrections which can be identified by the fact that other blocks become populated.

We thank A. Altland for discussions. This project has been funded by the Deutsche Forschungsgemeinschaft (DFG, German Research Foundation), Projektnummer 277101999, TRR 183 (project C01).

[1] M. Nakahara, *Geometry, Topology and Physics*, 2nd ed. (CRC press, 2003).
[2] F. Wilczek and A. Zee, Phys. Rev. Lett. **52**, 2111 (1984).
[3] D. Arovas, J. R. Schrieffer, and F. Wilczek, Phys. Rev. Lett. **53**, 722 (1984).
[4] X. G. Wen, Phys. Rev. Lett. **66**, 802 (1991).
[5] C. Nayak, S. H. Simon, A. Stern, M. Freedman, and S. Das Sarma, Rev. Mod. Phys. **80**, 1083 (2008).
[6] J. Pachos, P. Zanardi, and M. Rasetti, Phys. Rev. **A 61**, 010305(R) (1999).
[7] J. A. Jones, V. Vedral, A. Ekert, and G. Castagnoli, Nature **403**, 869 (2000).
[8] A. Zee, Phys. Rev. A **38**, 1 (1988).
[9] M. Z. Hasan and C. L. Kane, Rev. Mod. Phys. **82**, 3045 (2010).
[10] F. Yang and R.-B. Liu, Phys. Rev. B **90**, 245205 (2014).
[11] X. G. Wen, Rev. Mod. Phys. **89**, 041004 (2017).
[12] D. Xiao, M. C. Chang, and Q. Niu, Rev. Mod. Phys. **82**, 1959 (2010).
[13] K. Osterloh, M. Baig, L. Santos, P. Zoller, and M. Lewenstein, Phys. Rev. Lett. **95**, 010403 (2005).
[14] T. Li, L. Duca, M. Reitter, F. Grusdt, E. Demler, M. Endres, M. Schleier-Smith, I. Bloch, and U. Schneider, Science **352**, 1094 (2016).
[15] S. Carroll, *Spacetime and Geometry* (Addison-Wesley, 2003).
[16] M. V. Berry, Proc. R. Soc. London A **392**, 45 (1984).
[17] D. Ellinas, S. M. Barnett, and M. A. Dupertuis, Phys. Rev. A **39**, 3228 (1989).
[18] D. Gamliel and J. H. Freed, Phys. Rev. A **39**, 3238 (1989).
[19] F. Gaitan, Phys. Rev. A **58**, 1665 (1998).
[20] J. E. Avron and A. Elgart, Phys. Rev. A **58**, 4300 (1998).
[21] A. Carollo, I. Fuentes-Guridi, M.F. Santos, and V. Vedral, Phys. Rev. Lett. **90**, 160402 (2003).
[22] G. De Chiara and G. M. Palma, Phys. Rev. Lett. **91**, 090404 (2003).
[23] R. S. Whitney and Y. Gefen, Phys. Rev. Lett. **90**, 190402 (2003).
[24] R. S. Whitney, Y. Makhlin, A. Shnirman, and Y. Gefen, Phys. Rev. Lett. **94**, 070407 (2005).
[25] S. Syzranov and Y. Makhlin, *Electron Transport in Nanosystems*, p.301 (Springer, Dordrecht, 2008).
[26] S. Berger, M. Pechal, P. Kurpiers, A. A. Abdumalikov, C. Eichler, J. A. Mlynek, A. Shnirman, Y. Gefen, A. Wallraff, and S. Filipp, Nat. Commun. **6**, 8757 (2015).
[27] P. J. Leek, J. M. Fink, A. Blais, R. Bianchetti, M. Göppl, J. M. Gambetta, D. I. Schuster, L. Frunzio, R. J. Schoelkopf, A. Wallraff, Science **318**, 1889 (2007).
[28] K. Snizhko, R. Egger, and Y. Gefen, accompanying PRB submission.
[29] J. Alicea, Rep. Prog. Phys. **75**, 076501 (2012).
[30] R. M. Lutchyn, E. P. A. M. Bakkers, L. P. Kouwenhoven, P. Krogstrup, C. M. Marcus, and Y. Oreg, Nat. Rev. Mat. **3**, 52 (2018).
[31] U. Weiss, *Quantum Dissipative Systems*, 4th ed. (World Scientific, Singapore, 2007).
[32] We assume $\delta\boldsymbol{\lambda}(t=0,T)=0$. As long as Eq. (4) holds, however, this is not essential.
[33] For instance, $\delta_{\tau_c}(t)=e^{-|t|/\tau_c}/(2\tau_c)$, cf. Ref. [26].
[34] R. Horn and C. Johnson, *Matrix Analysis* (Cambridge University Press, Cambridge, England, 1985).
[35] R. Tycko, Phys. Rev. Lett. **58**, 2281 (1987).
[36] J. W. Zwanziger, M. Koenig, and A. Pines, Phys. Rev. A **42**, 3107 (1990).
[37] A. A. Abdumalikov Jr, J. M. Fink, K. Juliusson, M. Pechal, S. Berger, A. Wallraff, and S. Filipp, Nature **496**, 482 (2013).
[38] S. Murakami, N. Nagaosa, and S.-C. Zhang, Science **301**, 1348 (2003).
[39] J. D. Sau, D. J. Clarke, and S. Tewari, Phys. Rev. B **84**, 094505 (2011).
[40] B. van Heck, A. R. Akhmerov, F. Hassler, M. Burrello, and C. W. J. Beenakker, New J. Phys. **14**, 035019 (2012).
[41] T. Karzig, Y. Oreg, G. Refael, and M. H. Freedman, Phys. Rev. X **6**, 031019 (2016).
[42] A. Rahmani, B. Seradjeh, and M. Franz, Phys. Rev. B **96**, 075158 (2017).
[43] M. Cheng, V. Galitski, and S. Das Sarma, Phys. Rev. B **84**, 104529 (2011).
[44] C. Knapp, M. Zaletel, D. E. Liu, M. Cheng, P. Bonderson, and C. Nayak, Phys. Rev. X **6**, 041003 (2016).
[45] S. Plugge, A. Rasmussen, R. Egger, and K. Flensberg, New J. Phys. **19**, 012001 (2017).
[46] L. Fu, Phys. Rev. Lett. **104**, 056402 (2010).
[47] K. Flensberg, Phys. Rev. Lett. **106**, 090503 (2011).
[48] D. Aasen, M. Hell, R. V. Mishmash, A. Higginbotham, J. Danon, M. Leijnse, T. S. Jespersen, J. A. Folk, C. M. Marcus, K. Flensberg, and J. Alicea, Phys. Rev. X **6**, 031016 (2016).
[49] S. Plugge, L. A. Landau, E. Sela, A. Altland, K. Flensberg, and R. Egger, Phys. Rev. B **94**, 174514 (2016).
[50] T. Karzig, C. Knapp, R. M. Lutchyn, P. Bonderson, M. B. Hastings, C. Nayak, J. Alicea, K. Flensberg, S. Plugge, Y. Oreg, C. M. Marcus, and M. H. Freedman, Phys. Rev. B **95**, 235305 (2017).